Enabling tools for engineering collagenous tissues integrating bioreactors, intravital imaging, and biomechanical modeling

Laura E. Niklason[a,1], Alvin T. Yeh[b], Elizabeth A. Calle[a], Yuqiang Bai[b], Arturo Valentín[b], and Jay D. Humphrey[b]

[a]Department of Biomedical Engineering, Yale University, New Haven, CT 06520; and [b]Department of Biomedical Engineering, Texas A&M University, College Station, TX 77843

Edited by Robert Nerem, Georgia Institute of Technology, Atlanta, GA, and accepted by the Editorial Board October 22, 2009 (received for review July 13, 2009)

Many investigators have engineered diverse connective tissues having good mechanical properties, yet few tools enable a global understanding of the associated formation of collagen fibers, the primary determinant of connective tissue stiffness. Toward this end, we developed a biomechanical model for collagenous tissues grown on polymer scaffolds that accounts for the kinetics of polymer degradation as well as the synthesis and degradation of multiple families of collagen fibers in response to cyclic strains imparted in a bioreactor. The model predicted well both overall thickness and stress-stretch relationships for tubular engineered vessels cultured for 8 weeks, and suggested that a steady state had not yet been reached. To facilitate future refinements of the model, we also developed bioreactors that enable intravital nonlinear optical microscopic imaging. Using these tools, we found that collagen fiber alignment was driven strongly by nondegraded polymer fibers at early times during culture, with subsequent mechano-stimulated dispersal of fiber orientations as polymer fibers degraded. In summary, mathematical models of growth and remodeling of engineered tissues cultured on polymeric scaffolds can predict evolving tissue morphology and mechanics after long periods of culture, and related empirical observations promise to further our understanding of collagen matrix development in vitro.

collagen | connective tissue | optical microscopy | tissue engineering

Soft connective tissues, including skin, fascia, ligaments, tendons, and arteries, must withstand physical forces that result from physiological processes and diverse motions experienced in everyday life. Although contractile cells can help resist tensile loads in some connective tissues (e.g., arteries), most load-bearing is attributable to extracellular matrix (1–3). Collagen is the primary insoluble structural protein in the extracellular matrix and the single most abundant protein in the animal kingdom. Approximately 80–90% of collagen in humans exists in the fibrillar forms, types I, II, or III (4), with the major load-bearing function typically performed by type I, and, to a lesser extent, type III collagen (5). Many cell types increase collagen synthesis in response to mechanical stimuli (6, 7), but achieving normal load bearing capacity also depends on effective fibrillogenesis, which in turn is influenced by factors such as reticular collagens, proteoglycans, and cross-linking enzymes (8–10).

Despite having a detailed understanding of the molecular events of collagen assembly, our understanding of processes that govern the formation of bulk tissues remains wanting. To develop a better understanding of the genesis, development, and adaptability of soft connective tissues, it is necessary to go beyond the single molecule and to consider assemblies of cells and matrix working dynamically as a composite material. In this report, we describe progress in the development of specialized bioreactors, intravital imaging tools, and mathematical models that allow us both to track in real time and to predict collagen deposition during the development of engineered tissues. We focus on smooth muscle seeded engineered arteries for illustrative purposes, but the imaging tools and modeling principles can be extended to other collagen-producing cell types and tissues. The bioreactors were designed with optical-quality windows that allow nonlinear optical microscopic (NLOM) imaging of developing collagen fibers; they also enable the delivery of tightly controlled, mechanical cues (11). A mathematical model of polymer degradation and collagen deposition was also formulated to enable comparisons of predicted tissue mechanics and experimental measurements. Although still at an early stage, these evolving tools promise to aid greatly the engineering of diverse collagen-based connective tissues and thereby advance the field of regenerative medicine.

Results

Formulation of a Mathematical Model. Standard polyglycolic acid (PGA) has a modulus of elasticity ≈7 GPa, maximum, and an extensibility of 15–20% (12). Chemical pretreatments of PGA (e.g., immersion in 1.0 M NaOH) reduce its half-life to 25–35 days, shortening its load carrying capability to 20 days (13); this degradation can be captured via a first order kinetic model (14). Often seeded with $\approx 5 \times 10^6$ cells per mL, smooth muscle cell (SMC) density within PGA constructs can increase within just 8 weeks to $\approx 7.5 \times 10^7$ cells per mL, or 15-fold. Collagen content can increase from 0 to 45% (by dry weight), with orientations (primarily axial, circumferential, and helical) after 8 weeks of culture similar to those of native arteries (15, 16).

Classical equations of arterial mechanics are (linear momentum and constitutive, respectively)

$$div\mathbf{t} = \rho\mathbf{a}, \quad \mathbf{t} = 2\mathbf{F}\,\frac{\partial W}{\partial \mathbf{C}}\,\mathbf{F}^T - p\mathbf{I}, \qquad [1]$$

where $\mathbf{t}$ is the Cauchy (true) stress tensor, ρ is the mass density, $\mathbf{a}$ is the acceleration, $\mathbf{F}$ is the deformation gradient tensor, $\mathbf{C}$ (= $\mathbf{F}^T\mathbf{F}$) is the right Cauchy–Green tensor, $W(\mathbf{C})$ is the strain-energy, p is a Lagrange multiplier that enforces isochoric motions during transient loading, and $\mathbf{I}$ is the identity tensor. Because inertial loads are typically negligible, $\mathbf{a} \sim \mathbf{0}$ and deformations over the cardiac cycle can be treated as quasi-static (17).

To account for growth and remodeling (G&R), we assume that $k = 1, 2, \ldots, n$ structurally significant constituents can possess different natural (stress-free) configurations, material properties, and rates and extents of turnover, and yet be con-

Author contributions: L.E.N., A.T.Y., and J.D.H. designed research; E.A.C., Y.B., A.V., and J.D.H. performed research; A.T.Y., Y.B., and A.V. analyzed data; and L.E.N., A.T.Y., and J.D.H. wrote the paper.

Conflict of interest statement: L.E.N. has a financial interest in Humacyte, Inc., a regenerative medicine company. Humacyte, Inc. did not fund these studies, and Humacyte, Inc. did not affect the design, interpretation, or reporting of any of the experiments herein.

This article is a PNAS Direct Submission. R.N. is a guest editor invited by the Editorial Board.

[1]To whom correspondence should be addressed. E-mail: laura.niklason@yale.edu.

strained to move with the overall mixture (artery). That is, $\mathbf{x}^k \equiv \mathbf{x}$, thus deformation gradients experienced by individual constituents are $\mathbf{F}^k_{n(\tau)}(s) = \partial \mathbf{x}^k(s)/\partial \mathbf{X}^k(\tau) \equiv \partial \mathbf{x}(s)/\partial \mathbf{X}^k(\tau)$, where s denotes the current G&R time and $\tau \in [0, s]$ denotes the time at which constituent k was produced relative to its individual natural configuration. The energy stored in a tissue due to deformation may be written as the sum of energies stored in individual constituents, namely $W(\mathrm{s}) = \Sigma\, W^k(\mathbf{C}^k_{n(\tau)}(s))$. Because some constituents are continually produced and removed, we postulate that (18)

$$W^k(s) = \frac{\rho^k(0)}{\rho(s)}\, Q^k(s)\widehat{W}^k(\mathbf{C}^k_{n(0)}(s)) + \int_0^s \frac{m^k(\tau)}{\rho(s)}\, q^k(s-\tau)\widehat{W}^k(\mathbf{C}^k_{n(\tau)}(s))d\tau, \quad [2]$$

where $\rho^k(0)$ is the initial constituent mass density, $\rho(\mathrm{s}) = \Sigma\, \rho^k(s)$ is the overall mass density of the tissue, $Q^k(s) \in [0, 1]$ is the fraction of constituents produced before $s = 0$ that survive to current time s, $m^k(\tau) > 0$ is the true mass density production rate (e.g., matrix synthesis or cell proliferation), and $q^k(s - \tau) \in [0, 1]$ the fraction of constituents produced at a prior time τ that survives to current time s. Noting that $s = 0$ is the time at which G&R commences, the heredity integral contribution is similar to the concept of fading memory in nonlinear viscoelasticity; constituents typically contribute more to load bearing the more recently they were produced.

Similar to the form of Eq. **2**, mass balance for individual constituents can be accounted for via

$$\rho^k(s) = \rho^k(0)Q^k(s) + \int_0^s m^k(\tau)q^k(s-\tau)d\tau. \quad [3]$$

It can be shown that both at $s = 0$, and in the case of tissue maintenance (i.e., balanced production and removal of constituents), Eqs. **2** and **3** recover the usual rule of mixtures as they should: $W(s) = \Sigma\, \phi^k(s)\widehat{W}^k(s)$, where $\phi^k(s) = \rho^k(s)/\rho(s)$ denotes individual mass fractions and $\widehat{W}^k(s)$ are constituent-specific stored energy functions (18).

Hence, the general problem formulation reduces to solving quasi-static equilibria given constitutive relations for individual constituents: $\widehat{W}^k(s)$, $m^k(\tau)$, and $q^k(s - \tau)$. The G&R framework represented by Eqs. **1** to **3** can be adapted easily to describe the development of engineered collagenous tissues, with the primary need being to identify and implement appropriate constitutive relations for the evolving construct. For relations for tubular tissue initially consisting of cells seeded on PGA and subjected to cyclic strain, see *Materials and Methods*.

Modeling Results for Engineered Tubular Tissues. Fig. 1*A* shows that the simulated engineered vessel was predicted to atrophy as the PGA degraded and then to thicken as SMC proliferated and increased their synthesis of collagen. If one assumed that basal collagen production rates, comparable with native tissues, were achieved by the end of the 8-week culture period, then the model (dashed curve) under-predicted measured values (≈0.3 mm) of wall thickness (19, 20). If, instead, the basal rate was chosen to yield the correct wall thickness at 8 weeks (solid curve), then the model predicted that steady state turnover would not be achieved within 8 weeks. Empirical observations of engineered vessels (19, 20) suggest that rates of collagen production and cell division are much higher in the engineered tissues than in mature native arteries.

Fig. 1*B* shows that the predicted mechanical behavior transitioned quickly from that of a stiff PGA polymer (classical neo-Hookean type response) to that of a soft tissue (Fung-type exponential). Because mechanical properties of PGA scaffolds are negligible after 3 weeks (13), while collagen accumulates throughout the culture period (16, 19), this result seems reasonable. More importantly, the predicted mean circumferential Cauchy stress-stretch behavior at 8 weeks was very similar to that observed for engineered arteries cultured for 7.5 weeks under cyclic strains (Fig. 1*C*) (21). This good agreement between predicted and empirical findings suggests that the basic model can capture salient aspects of collagen deposition and organization after long culture periods.

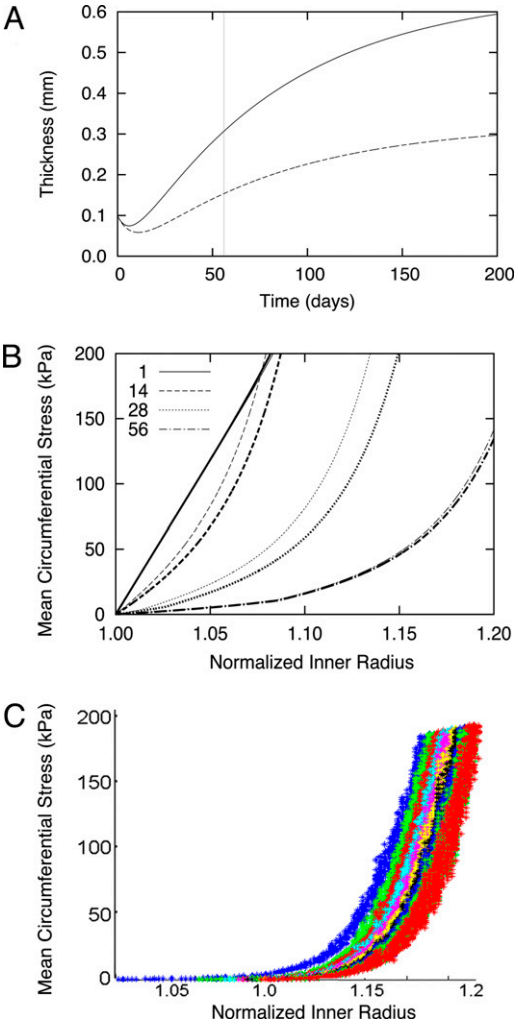

Fig. 1. Results from modeling and experiments for tubular constructs cultured at $\Lambda_\theta = 1.015$ and $\Lambda_z = 1.00$; results were similar for $\Lambda_z = 1.015$ or 1.03. (*A*) Predicted time course of construct thickness during culture for $f = 90$ beats per minute (bpm); results were similar for 180 bpm. The dashed line shows results based on the assumption that a steady state turnover was achieved at 8 weeks, whereas the solid line shows results based on the assumption that the construct reached its actual thickness at 8 weeks. (*B*) Evolving circumferential Cauchy stress-stretch behavior for the theoretical engineered vessel. Light curves show results for $f = 90$ bpm, whereas dark curves show results for 180 bpm. Note that effects of frequency were predicted to be modest, consistent with previous experimental observations (37, 43). (*C*) Measured stress-stretch data for an actual engineered vessel after 7.5 weeks of culture (data from ref. 21), showing 10 cycles of inflation from 0–120-mm Hg. Note the similarity in overall behavior to the predicted behavior in *B* and that the model was not designed to account for preconditioning effects.

Collagen Fibers Observed Using NLOM. To better understand and quantify the formation of collagen fibers during culture, vessels

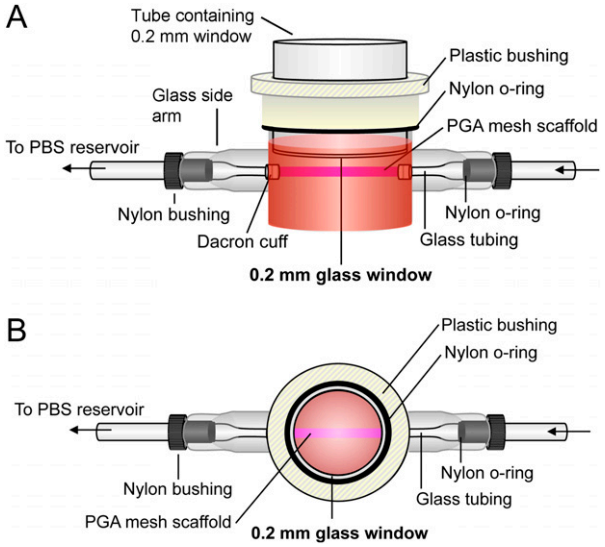

Fig. 2. Imaging bioreactor for vessel culture. Imaging window can slide up and down such that the optical glass can be brought into direct contact with the engineered tissue. Side (*A*) and top (*B*) views.

were grown in redesigned bioreactors having optical windows that enable direct observation of construct architecture (Fig. 2). Vessels were imaged at select times during the 8-week culture period to construct a time course of collagen fiber deposition and alignment. Whereas we did not monitor individual constructs throughout culture, the bioreactors were designed to interface with the NLOM system without compromising sterility, thereby enabling future serial measurements.

Strong two-photon excited fluorescence (TPF), arising from PGA and cells, and second harmonic generation (SHG), arising from collagen, were spectrally distinct. Representative images at depths of 30–135 μm are shown in Fig. 3 *A–D*. Distributions of collagen fiber orientations were calculated from SHG images using Fourier analysis and custom software (Continuity, courtesy of A. D. McCulloch, University of California at San Diego, La Jolla, CA). Quantification included an Alignment Index (AI), which is defined as the fraction of collagen fibers oriented within 20° of a predominant direction and ranges from random (1.0) to strong (4.6) alignment (22). At 2 weeks of culture, collagen was adjacent to seeded cells and PGA fibers, although the sparseness of collagen and noncompacted nature of the PGA scaffold precluded accurate computation of an average fiber alignment (Fig. 3*A*). At 4 weeks, considerably more collagen had been deposited and aligned along remaining PGA fibers, thus revealing one effect of scaffold fibers on collagen deposition (Fig. 3*B*). Collagen alignment was particularly noticeable in outer layers of the construct, coincident with polymer fibers.

At 6 weeks of culture (Fig. 3*C*), collagen density had increased, and so too the dispersion of orientation angles. This increased dispersion likely reflected both a waning influence of the degrading PGA in directing collagen orientation and an increased significance of cellular responses to mechanical stimuli applied by the bioreactor. These trends continued at 8 weeks (Fig. 3*D*), thus suggesting a progressively increasing distensibility (see Fig. 1*C*) and near isotropy.

A cumulative plot of collagen fiber orientations throughout the wall of the 8-week construct (Fig. 3*E*) was consistent with alignment of four predominant "families" within the image plane. Collagen fiber families were centered approximately at 0°, ±45°, and 90° (note, the 90° family wraps approximately from +90° to −90°). These orientations are consistent with our prior observations of collagen fibers in engineered vessels by transmission electron microscopy (15) and with model predictions, i.e., the model predicted that mass fractions for the four primary families of collagen fibers evolved to comparable values at 8 weeks (≈33% axial, ≈37% circumferential, and ≈30% for the axially symmetric helical families); thus suggesting a near isotropy in bulk behavior, as might be expected given the culture conditions of cyclic circumferential stretches from 1.0 to 1.015 and constant axial stretches of 1.0.

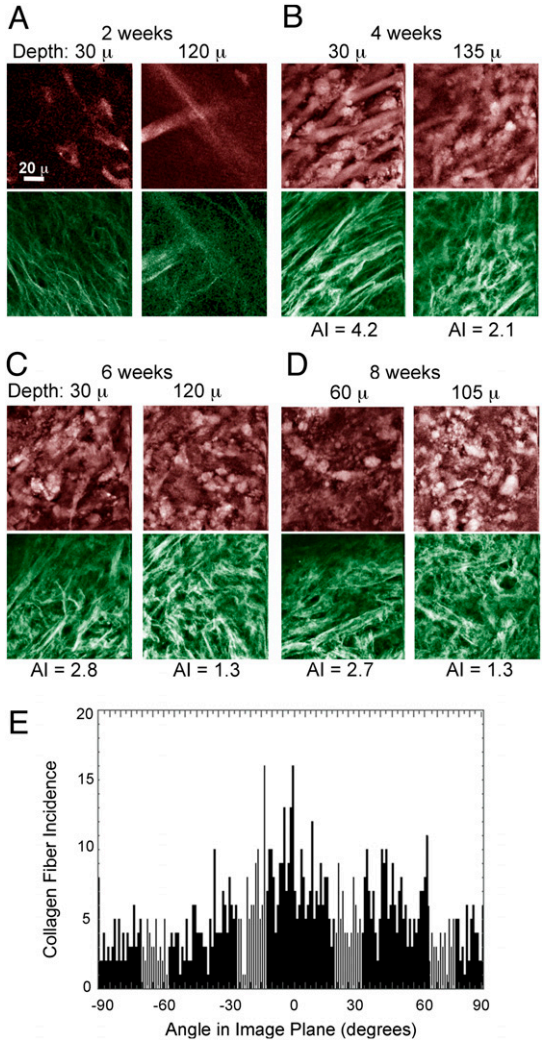

Fig. 3. NLOM imaging of constructs from 2–8 weeks of culture. Pseudocolored images of PGA polymer and cellular material (red panels) and collagen fibers (green panels). (*A* and *B*) Fibers of PGA scaffold were clearly visible at 2 and 4 weeks, with collagen deposition running parallel to PGA fibers. (*B–D*) Local collagen alignment with PGA fibers decreased as the PGA degraded, as revealed by the AI computed for the collagen fibers at weeks 4–8. Depth of image acquisition into the vessel wall is shown in micrometers. (Scale bar in *A Upper Left* applies to all images.) (*E*) Projection of all collagen fiber angles from 8-week specimen.

Discussion

Progress in tissue engineering has been significant over the past two decades, with most attention focused on biochemical culture conditions, cellular interactions with synthetic matrices, and the like (23). Nevertheless, these efforts alone have not led to many clinical successes in connective tissue replacement. For many tissues, such as skin, ligament, tendon, and arteries, synthetic materials or native tissues are still the mainstays of therapy

because engineered tissues do not have sufficient tensile strength to function properly in vivo (24–26). Even in instances where strong tissues have been generated (19, 27, 28), we have only a limited understanding as to how and why such improvements have been realized. Without noninvasive, serial assessments of extracellular matrix development, combined with a unifying conceptual understanding of matrix deposition and organization, our path to understanding the impact of culture conditions on matrix deposition and mechanics will continue to be slow.

The present model predictions of overall vessel morphology and mechanics agreed well with experiment at 8 weeks of culture, thus suggesting that it is possible to establish a mathematical framework for predicting and understanding the development of engineered collagenous matrix. In addition, the model predicted the development of four families of collagen fibers that were consistent with observations from NLOM and prior measurements by transmission electron microscopy. Nevertheless, there is a need to refine the model based on additional data. For example, NLOM imaging showed that during early periods of culture, collagen fiber alignment largely paralleled the orientation of PGA fibers, which possessed an aggregate alignment based upon the method of manufacture of the mesh scaffold. Because PGA fibers are only 13 μm in diameter, whereas the long axis of an SMC can be >50 μm, it is likely that adherent SMC extended along the long axis of the PGA fibers. Several investigators have shown that collagen-producing cells secrete collagen along their long axes (29, 30); hence cellular alignment along PGA fibers may have "forced" the direction of collagen fiber deposition, at least at early times during culture before the PGA fibers degraded. Only after the scaffold fibers degraded did SMC presumably reorient consistent with macroscopic stress or strain fields and then deposit collagen fibers along directions dictated by applied loads.

There is need to understand more fully the transition from scaffold architecture-dominated to load-dominated organization of deposited collagen fibers, including radial gradients therein. We also need to understand better how nonequibiaxial stress or strain fields dictate the orientation of subsequently synthesized collagen. Finally, there is a need to understand better the effects of different additives in the culture medium, which has been tailored to maximize collagen synthesis, thereby resulting in collagen deposition rates that are far greater than those typically observed in vivo. In other words, we must increase our understanding and incorporation of chemo-mechanical stimuli on the matrix deposition by connective tissue cells.

Our results show further that nondestructive, high-resolution NLOM offers complementary information to traditional histochemical-based assessments of developing tissue-engineered constructs. NLOM accesses a wealth of nonlinear optical signals that are specific to biological molecules and their chemical environments (31–33). Coincidence of collagen deposition with PGA fibers was highlighted in NLOM by constituent-specific, endogenous signals (SHG and TPF, respectively) (34–36). NLOM is particularly sensitive to the extracellular matrix, especially fibrillar collagens and mature elastin, without the use of exogenous labels. These attributes make NLOM well suited for serial measurements of engineered constructs during culture. Associated quantification of evolving distributions of collagen fibers promise to enable refinements in the modeling, thus permitting iterative improvements in theory-based design of culture conditions.

In summary, we have described mathematical modeling approaches and imaging techniques that allow us to predict, track, and quantify collagenous extracellular matrix production in engineered tissues. Although the specific model tissue discussed here was tubular and grown from an SMC-seeded PGA scaffold, both the modeling framework and the imaging strategies could be adapted to other connective tissues and cell types. Guided by further experimentation and imaging, we expect that mathematical models for evolving connective tissue mechanics will continue to be refined, thereby enhancing our global understanding of connective tissue regeneration.

Materials and Methods

Predictive Model for Engineered Tissues. We assumed that the primary tensile load-bearing constituents are the synthetic PGA, which degrades over time, fibrillar collagen ($k = c$), and passive smooth muscle ($k = m$). Associated stored energy functions were assumed to be of neo-Hookean and exponential forms,

$$\widehat{W}^{\mathrm{PGA}}(s) = c^{\mathrm{PGA}}((\lambda_\theta^{\mathrm{PGA}})^2 + (\lambda_z^{\mathrm{PGA}})^2 + \frac{1}{(\lambda_\theta^{\mathrm{PGA}}\lambda_z^{\mathrm{PGA}})^2} - 3), \quad \textbf{[A1]}$$

$$\widehat{W}^{k}(s) = \frac{c_1^k}{4c_2^k}\left(\exp\left[c_2^k\left(\lambda_{n(\tau)}^k(s)^2 - 1\right)^2\right] - 1\right), \quad \textbf{[A2]}$$

where c_i^k ($k = c$ or m) are material parameters. Individual fiber stretches are related easily to overall tissue stretches Λ_θ and Λ_z via (18)

$$\lambda_{n(\tau)}^k(s) = G_h^k\frac{\sqrt{\Lambda_z^2(s)\cos^2\alpha_0^k + \Lambda_\theta^2(s)\sin^2\alpha_o^k}}{\sqrt{\Lambda_z^2(\tau)\cos^2\alpha_0^k + \Lambda_\theta^2(\tau)\sin^2\alpha_o^k}} \quad \textbf{[A3]}$$

where G_h^k are values at which fibers are incorporated within extant matrix, and α_o^k are angles between fiber orientations and the z-direction in the original unloaded configuration. Here, the former were assumed to be similar to those in native arteries, hence $G_h^c \sim 1.08$ and $G_h^m \sim 1.20$; the latter were assumed to represent axial (0 radians), circumferential ($\pi/2$ radians), and symmetric helical ($\pm\pi/4$ radians) fibers, consistent with our previous observations (15). Hence, the overall material symmetry of the growing tissue was modeled via changing distributions of fibers, i.e., the combination of unloaded orientations and evolving mass fractions for the individual families of fibers. Note, too, that the fibers were allowed to reorient affinely during deformation so as to account for any load-induced changes in anisotropy.

With regard to material properties, we let $c^{\mathrm{PGA}} \sim 6$ GPa (12) as well as (c_1^c, c_2^c) = (560.4 kPa, 22) for all four families of collagen fibers and (c_1^m, c_2^m) = (36.5 kPa, 3.5) for passive SMC (18). Although changes in collagen cross-linking can be accounted for by evolving c_1^c, we recently found no significant difference in cross-link density at 7 weeks due to pulsatile stimuli (37), and thus did not attempt to model changing cross-links. Obviously, values for other specific polymer scaffolds and cell types may be incorporated to fit different experimental scenarios. Because the contractile capacity of SMC in engineered vascular tissues is only ≈1.5% of native (16), SMC contractility was ignored, thereby rendering the cellular elements similar to fibroblasts or other noncontractile mesenchymal cells for purposes of this model.

At time $s = 0$, the construct consists solely of PGA scaffold and seeded cells that were assumed not to bear load (i.e., $\phi^{\mathrm{PGA}}(0) = 1$). The PGA degrades thereafter, hence

$$\phi^{\mathrm{PGA}}(s) = \phi^{\mathrm{PGA}}(0)\exp\left[-k_q^{\mathrm{PGA}}s\right] \quad \textbf{[A4]}$$

where $k_q^{\mathrm{PGA}} \sim 1/10$ day^{-1} (13). A candidate model for capturing collagen production is*

$$m^c(\tau) = m^c_{\mathrm{basal}}\xi^m(\tau)\left(1 + K_\omega\left(\frac{\omega(\tau) - \omega_h}{\omega_h}\right)\right) \cdot\left(1 + K_\lambda^c\left(\frac{\lambda^c(\tau) - G_h^c}{G_h^c}\right)\right), \quad \textbf{[A5]}$$

where $\xi^m(\tau)$ captures an increasing synthetic capability due to early proliferation of SMC, which was modeled as simple exponential growth $\xi^m(\tau) = 1 - \exp[-\kappa\tau]$ with $\kappa = 0.2$ day^{-1} (39). Initial values for the gain-type parameters were $K\omega = 0.5$ and $K_\lambda^c = 10$, with $\omega_h = 2\pi(90)$, but these values can be tuned depending on experimental findings.

*Most prior models of arterial growth and remodeling employ stress as a convenient metric for driving turnover, but the presence of the inner silicone tube renders calculation of wall stress less clear in these PGA-based systems; hence, cyclic stretch was used as the metric because of its ease of measurement in vitro; see ref. 38.

Collagen removal was assumed to follow first-order kinetics, hence

$$q^c(s,\tau) = \exp\left(\int_\tau^s -K_q^c(\tilde{\tau})d\tilde{\tau}\right), \qquad \text{[A6]}$$

where K_q^c ranges from ~1/80 day^{-1} in normal arteries to ~1/8 day^{-1} in extreme hypertension. Finally, for purposes of simulation, we let the original radius, wall thickness, and length be A (0) = 3.0 mm, H (0) = 0.1 mm, and L (0) = 70 mm (13), although these may be tailored as well. Baseline values of the imposed overall stretches were Λ_θ = 1.015 and Λ_z = 1.00, consistent with typical prescribed loading conditions (21).

Vessel Culture for Mechanical Testing. The bioreactor systems, cell seeding, and medium replenishment proceeded as described previously (21). Vessels cultured for 7.5 weeks under pulsatile conditions were subjected to biaxial mechanical testing, with axial length fixed at the length of the vessel in the bioreactor, as described previously (21). Vessels were cyclically inflated from 0 to 120 mmHg over 10 cycles, and strain was recorded by tracking the movements of markers placed on the vessel surface.

Imaging Bioreactor Preparation and Assembly. Glass bioreactors were hand-blown having side-arms to allow flow of perfusion fluid, and a top opening to allow placement of an occlusive cap or an imaging window (Fig. 2). The bioreactor arms were sealed with nylon *o*-rings and bushings having a 7.5-mm ID hole in the center (Ace Glass). The imaging window was constructed from a 3-cm glass tube fitted with a piece of 0.2-mm thickness optical glass at the bottom. The glass imaging tube was positioned inside a silicone bushing that was threaded into the top of the bioreactor and sealed with a silicone *o*-ring. The bushing and *o*-ring were designed such that the imaging tube could slide up and down in sterile fashion, thereby allowing the imaging window to be brought close to the engineered vessel for image acquisition, then retracted for resumption of culture.

Biodegradable PGA scaffolding (Concordia Fibers) was prepared in tubular form and treated with 1.0 M NaOH as described previously (20, 40). PGA fibers in the mesh scaffolding have some aggregate alignment due to the manufacturing processes used to make the nonwoven mesh (41). Silicone tubing having an OD of 3.1 mm and known compliance (Saint Gobain Performance Plastics) was threaded through the lumen so that applied cyclic pressurization of the tubing resulted in known radial distensions of the construct.

Vessel Culture in Imaging Bioreactor. Bovine aortic SMC, passage 3, were cultured in DMEM (Gibco) with 10% FBS and 1% penicillin-streptomycin. PGA scaffolds were seeded with a cell solution of 3 to 6×10^6 cells per mL; cells were allowed to adhere for 30 min, after which the bioreactor was filled with medium, as described previously (20). Vessels were cultured in the bioreactors for 2–8 weeks. Pulsatile flow of buffer was provided via a perfusion system to distend the silicone tubing ≈1.5% at ≈150 beats per minute (20). The full volume of medium in the bioreactor was replaced, or ascorbic acid was added to the medium at 0.05 mg/mL, every 2 or 3 days.

Noninvasive Imaging. The NLOM system has been described previously (42). Briefly, sub-10-fs pulses, with center wavelength of 800 and 130 nm of bandwidth from a Kerr-lens modelocked Ti:Al_2O_3 oscillator pumped by a frequency doubled solid state Nd:YVO_4 laser, were coupled to the epifluorescence port of an upright microscope by dual axis galvanometer mirrors. Imaging signals were collected by the focusing objective (backreflected geometry), separated from backscattered laser light by a short pass dichroic mirror, and directed to a two-channel photomultiplier tube based photon-counting detection system. Appropriate dichroic mirrors and bandpass filters were used to selectively detect SHG from collagen and TPF from PGA and cells. Custom software developed on Labview platform rendered 256×256 images as fast as 1 Hz, but typical acquisition rates used here were eight times slower.

ACKNOWLEDGMENTS. We thank Dr. Shannon Dahl for mechanical data. This work was supported by National Institutes of Health Grant R01 EB-008836.

1. Lanir Y (1983) Constitutive equations for fibrous connective tissues. *J Biomech* 16:1–12.
2. Armentano RL, et al. (1991) Assessment of elastin and collagen contribution to aortic elasticity in conscious dogs. *Am J Physiol* 260:H1870–H1877.
3. Pachence JM (1996) Collagen-based devices for soft tissue repair. *J Biomed Mat Res* 33:35–40.
4. Kucharz EJ (1992) *The Collagens: Biochemistry and Pathophysiology* (Springer, New York).
5. Alberts B (1994) *Molecular Biology of the Cell* (Garland Science, New York), 4th Ed.
6. Li Q, Muragaki Y, Hatamura I, Ueno H, Ooshima A (1998) Stretch-induced collagen synthesis in cultured smooth muscle cells from rabbit aortic media and a possible involvement of angiotensin II and transforming growth factor-beta. *J Vasc Res* 35:93–103.
7. Iversson M, McWhirter A, Borg TK, Rubin K (1998) Type I collagen synthesis in cultured human fibroblasts: Regulation by cell spreading, platelet-derived growth factor and interactions wtih collagen fibers. *Mat Biol* 16:409–425.
8. Wenstrup RJ, et al. (2006) Murine model of the Ehlers-Danlos Syndrome: Col5a1 haploinsufficiency disrupts collagen fibril assembly at multiple stages. *J Biol Chem* 281:12888–12895.
9. Heegaard A-M, et al. (2007) Biglycan deficiency causes spontaneous aortic dissection and rupture in mice. *Circulation* 115:2731–2738.
10. Takaluoma K, et al. (2007) Tissue specific changes in the hydroxylysine content and cross-links of collagen and alteration in fibril morphology in lysyl hydroxylase 1 knock-out mice. *J Biol Chem* 282:6588–6589.
11. Humphrey JD (2008) Vascular adaptation and mechanical homeostasis at tissue, cellular and sub-cellular levels. *Cell Biochem Biophys* 50:53–78.
12. Middleton JC, Tipton AJ (2000) In situ gelling systems to deliver peptides and proteins. *Biomaterials* 21:2335–2346.
13. Prabhakar V, et al. (2003) Porcine Engineered Arteries: Effects of Scaffold Modification. *J Biomed Mat Res* 67A:303–311.
14. Wilson CG, Bonassar LJ, Kohles SS (2002) Modeling the dynamic composition of engineered cartilage. *Arch Biochem Biophys* 408:246–254.
15. Dahl SLM, Vaughn ME, Niklason LE (2007) An ultrastructural analysis of collagen in tissue engineered arteries. *Ann Biomed Eng* 35:1749–1755.
16. Dahl SLM, Rhim C, Song YC, Niklason LE (2007) Mechanical properties and compositions of tissue engineered and native arteries. *Ann Biomed Eng* 35:348–355.
17. Humphrey J, Rajagopal K (2002) A constrained mixture model for growth and remodeling of soft tissues. *Math Model Meth Appl Sci* 12:407–430.
18. Valentin A, Cardamone L, Baek S, Humphrey JD (2009) Complementary vasoactivity and matrix turnover in arterial adaptations to altered flow and pressure. *J Royal Soc Interface* 6:293–306.
19. Niklason LE, et al. (1999) Functional arteries grown in vitro. *Science* 284:489–493.
20. Niklason LE, et al. (2001) Morphologic and mechanical characteristics of bovine engineered arteries. *J Vasc Surg* 33:628–638.
21. Dahl SL, et al. (2008) A microstructurally motivated model of the mechanical behavior of tissue engineered blood vessels. *Ann Biomed Eng* 36:1782–1792.
22. Hu J-J, Humphrey JD, Yeh AT (2009) Characterization of enginered tissue development under biaxial stretch using nonlinear optical microscopy. *Tiss Eng Part A* 15:1553–1564.
23. Guilak F, Butler DL, Goldstein SA, Mooney DJ (2003) *Functional Tissue Engineering* (Springer, New York).
24. Rao I, Humphrey J, Rajagopal K (2003) Biological growth and remodeling: A uniaxial example with possible application to tendons and ligments. *Comp Mod Engr Sci* 4:439–455.
25. Naughton G (1999) Skin: The first tissue-engineered products. The Advanced Tissue Sciences story. *Sci Am* 280:84–85.
26. Schechner JS, et al. (2003) Engraftment of a vascularized human skin equivalent. *FASEB J* 17:2250–2256.
27. L'Heureux N, Paquet S, Labbe R, Germain L, Auger FA (1998) A completely biological tissue-engineered human blood vessel. *FASEB J* 12:47–56.
28. L'Heureux N, et al. (2006) Human tissue-engineered blood vessels for adult arterial revascularization. *Nature Med* 12:361–365.
29. Richardson SH, et al. (2007) Tendon development requires regulation of cell condesnation and cell shape via cadherin-11-mediated cell-cell junctions. *Mol Cell Biol* 27:6218–6228.
30. Wang H, Layton BE, Sastry AM (2003) Nerve collagens from diabetic and nondiabetic Sprague-Dawley and biobreeding rats: An atomic force microscopy study. *Diab Metab Res Rev* 19:288–298.
31. Zipfel WR, Williams RM, Webb WW (2003) Nonlinear magic: Multiphoton microscopy in the biosciences. *Nature Biotech* 21:1369.
32. Campagnola PJ, Loew LM (2003) Second-harmonic imaging microscopy for visualizing biomolecular arrays in cells, tissues and organisms. *Nature Biotech* 21:1356.
33. Theer P, Hasan MT, Denk W (2003) Two-photon imaging to a depth of 1000 microns in living brains by use of a Ti:Al2O3 regenerative amplifier. *Opt Lett* 28:1022.
34. Squier JA, et al. (1998) Third harmonic generation microscopy. *Opt Express* 3:315–324.
35. Theodossiou TA, Thrasivoulou C, Ekwobi C, Becker DL (2006) Second harmonic generation confocal microscopy of collagen type I from rat tendon cryosection. *Biophys J* 91:4665.
36. Nadiarnykh O, LaComb R, Campagnola PJ, Mohler WA (2007) Coherent and incoherent SHG in fibrillar cellulose matrices. *Opt Express* 15:3348.
37. Solan A, Dahl SL, Niklason LE (2009) Effects of mechanical stretch on collagen and cross-linking in engineered blood vessels. *Cell Transpl*, in print.
38. Humphrey JD (2001) Stress, strain and mechanotransduction in cells. *J Biomech Eng* 123:638–641.
39. Bailey JE, Ollis DF (1977) *Biochemical Engineering Fundamentals* (McGraw-Hill, New York).
40. Gao J, Niklason LE, Langer RS (1998) Surface modification of polyglycolic acid meshes increases the seeding density and spreading of smooth muscle cells. *J Biomed Mat Res* 42:417–424.
41. Freed LE, et al. (1994) Biodegradable polymer scaffolds for tissue engineering. *BioTechnol* 12:689–693.
42. Larson AM, Yeh AT (2006) Ex-vivo characterization of sub-10-fs pulses. *Opt Lett* 31:1681.
43. Solan A, Mitchell S, Moses M, Niklason L (2003) Effect of pulse rate on collagen deposition in the tissue-engineered blood vessel. *Tiss Eng* 9:579–586.